

Synthesis and Photocatalytic Properties of Sol-Gel Derived B₂O₃-SiO₂-TiO₂ Glass-Ceramic Coatings

Yasser MoradHaseli¹, Bijan Eftekhari Yekta¹, Alireza Mirhabibi², Sara Ahmadi^{3,*}

¹Ceramic Division, School of Materials and Metallurgy Engineering, Iran University of Science and Technology, Tehran, Iran

²School of Chemical and Process Engineering, University of Leeds, Leeds, LS2 9JT

³ Construction and Minerals Research Group, Technology and Engineering Research Center, Standard Research Institute, Karaj, Alborz, Iran
s.ahmadi@standard.ac.ir

Abstract

The crystallization behavior and photocatalytic properties of the sol-gel derived glass ceramic coatings in the TiO₂-SiO₂-B₂O₃ system were studied. The prepared sol was sprayed on a glazed ceramic wall. Following drying, the coated specimens were fired at 900°C for 1 h. The impact of boron oxide content in the composition was explored in terms of anatase stability and glass maturing temperature. The thermal and crystallization behaviors of the dried gels were studied by the STA, XRD, and FESEM. The photocatalytic property of the coated layer was examined using methylen blue degradation. Based on the results, the sample containing 15 wt% of boron oxide demonstrated about 30% dye removal efficiency, after only 60 min of UV-irradiation. Additionally, this particular sample exhibited the greatest magnitude of the anatase phase in comparison to the other samples.

Keywords: sol-gel, photocatalyst, glass-ceramic coating, anatase

1. Introduction

Nowadays, air and water pollution have become among the most critical environmental challenges. One promising solution involves the use of photocatalytic materials such as TiO₂, ZrO₂, ZnO, and CdS [1]. Among these, titanium dioxide (TiO₂) stands out due to its strong oxidation potential and remarkable hydrophilicity, enabling its application in air purification, deodorization, sterilization, and self-cleaning surfaces [2,3]. In contrast, alternative systems such as ZnO, while possessing similar band gaps to TiO₂, suffer from photocorrosion under UV irradiation. CdS, another potential candidate, is limited by its toxicity and instability under light exposure. ZrO₂, though chemically stable, has a wider band gap, reducing its photocatalytic efficiency under UV light [1-3].

The photocatalytic performance of TiO_2 is influenced by several factors, including its crystal structure, morphology, surface area, porosity, and pore distribution [4–6]. TiO_2 occurs in three polymorphs: brookite, anatase, and rutile. While anatase demonstrates the highest photocatalytic activity, it irreversibly transforms to rutile at temperatures between 500–600 °C [3–5].

To enhance the performance and stability of TiO_2 , many studies have focused on modifications such as doping or the use of fluxing agents. For example, Jung et al. demonstrated that B_2O_3 flux improves TiO_2 crystallinity while preserving the anatase phase [7], a finding supported by other researchers [8,9]. Additionally, incorporating silica has been shown to enhance both the thermal stability of the anatase phase and its photocatalytic efficiency [1,3,10–14].

Resende et al. [15] demonstrated that $\text{TiO}_2/\text{SiO}_2\text{--}\text{B}_2\text{O}_3$ ternary nanocomposites exhibit superior photocatalytic activity compared to commercial TiO_2 , attributing this enhancement to the unique interfacial properties introduced by B_2O_3 . Furthermore, Bachvarova-Nedelcheva et al. [16] reported that the inclusion of B_2O_3 in TiO_2 -based systems not only stabilizes the anatase phase but also imparts antibacterial properties, expanding the material's applicability.

Consequently, the $\text{B}_2\text{O}_3\text{--}\text{SiO}_2\text{--}\text{TiO}_2$ system was selected for this study due to its synergistic properties that enhance photocatalytic performance and offers a balanced combination of stability, safety, and enhanced photocatalytic performance, making it a superior choice for environmental applications.

A critical factor in practical applications is the durability of photocatalytic TiO_2 coatings. Conventional coatings often suffer from weak adhesion to glazed surfaces, limiting their longevity. In contrast, TiO_2 -based glass-ceramic layers have exhibited superior bonding and durability. The enhanced adhesion and durability of TiO_2 -based glass-ceramic coatings, compared to conventional TiO_2 layers, can be attributed to several interrelated factors. First, the glass-ceramic matrix allows for the formation of strong chemical bonds (e.g., Si--O--M and Ti--O--M , where M is a metal from the substrate) at the interface with the glazed substrate, which significantly surpasses weak van der Waals interactions typical of conventional coatings. Moreover, the coefficient of thermal expansion (CTE) of glass-ceramic systems can be tailored to better match that of the glazed surface, reducing thermal mismatch stress during firing and cooling. Also, partial softening of the glassy phase during sintering enables mechanical interlocking as the coating partially penetrates surface irregularities, anchoring it more securely. Furthermore, the in-situ crystallization of nanometric anatase crystals within the glassy matrix improves the mechanical stability and resistance to cracking or delamination.

Finally, the embedding of TiO₂ particles in a glassy network provides environmental protection, particularly against moisture and UV-induced degradation, thereby improving long-term performance. These synergistic effects, as supported by references [17] and [18], explain the superior bonding strength and durability observed in glass-ceramic TiO₂ coatings.

TiO₂ also serves as a nucleating agent in the fabrication of glass ceramics, facilitating controlled crystallization and enabling the production of materials with desirable crystallite sizes and microstructures [19]. These glass ceramics are valued for their cost-effectiveness, ease of shaping, and versatility in forms such as sheets, rods, tubes, and fibers, making them suitable for photocatalytic applications.

Recent research has explored TiO₂-containing glass ceramics as photocatalytic materials. For instance, Yazawa et al. synthesized rutile-type glass ceramics from silicate glasses [20-21], while other studies have successfully derived anatase-type glass ceramics from phosphate glasses [22]. These materials exhibited photocatalytic activity, as evidenced by methylene blue degradation under UV light [23].

In this study, anatase-phase TiO₂ was precipitated within a SiO₂-TiO₂-B₂O₃ glass layer via heat treatment of sol-gel-derived glass. The photocatalytic activity of the resulting glass-ceramic layer was quantitatively evaluated.

2.Experimental Procedure

2.1.materials and Sample preparation

the borosilicate glasses in the SiO₂-B₂O₃-TiO₂ system were prepared with sol gel method from reagent grade chemicals consisted of tetraethyl orthosilicate (TEOS, (Si (OC₂H₅)₄, Merck 800658), Titanium tetraisopropoxide (TTIP, Ti(OC₃H₇)₄, Merck 8251895), trimethyl borate (B(OC₂H₅)₃, Merck 82180), isopropanol (IPA ,Merck 109634), ethanol (EtOH,Merck 100983); Hydrochloric acid (37% solution,Merck 100317), and deionized water.

The nominal chemical compositions of the synthesized glass-ceramics are presented in table 1.

Table 1. The nominal chemical compositions of the glasses

| Composition | SiO ₂ (wt%) | B ₂ O ₃ (wt%) | TiO ₂ (wt%) |
|-------------|------------------------|-------------------------------------|------------------------|
| ST-5B | 30 | 5 | 65 |
| ST-10B | 30 | 10 | 60 |
| ST-15B | 30 | 15 | 55 |

Preparation of the sols were initiated by dissolution of TEOS in ethanol (1:4 molar ratios) and TTIP in isopropanol (1:4 molar ratios). The Si and Ti alkoxides hydrolyzed by adding 1 M HCl

as a catalyst. Following a 2 h stirring, the solution of Ti-tetraisopropoxide in isopropanol alcohol was added dropwise to the TEOS sol. The resulted solution was stirred until a transparent and solid free solution was achieved. Then, trimethyl borate with stoichiometric amount of water was added to alkoxides solution.

To ensure thorough hydrolysis of the alkoxides, the water content of the final solution was raised to twice the stoichiometric quantity and then agitated for 3 h. The final Titania-Silica-Borate sols were completely transparent without any precipitation. The prepared sols were applied on the glazed ceramic tile by a spraying process. The coated tiles were dried at 150 °C for 24 h and then heat treated of at various temperatures to prepare glass ceramic. The heating rate was 10 °C /min. Fig. 1 depicts the flowchart of gel preparation procedure.

Methylene blue (MB,159270) with chemical formula $C_{16}H_{18}ClN_3S \cdot nH_2O$ ($n=2-3$) was employed as the representative pollutant to study the photocatalytic properties of the prepared glass-ceramic layers coated on the glazed ceramic tiles.

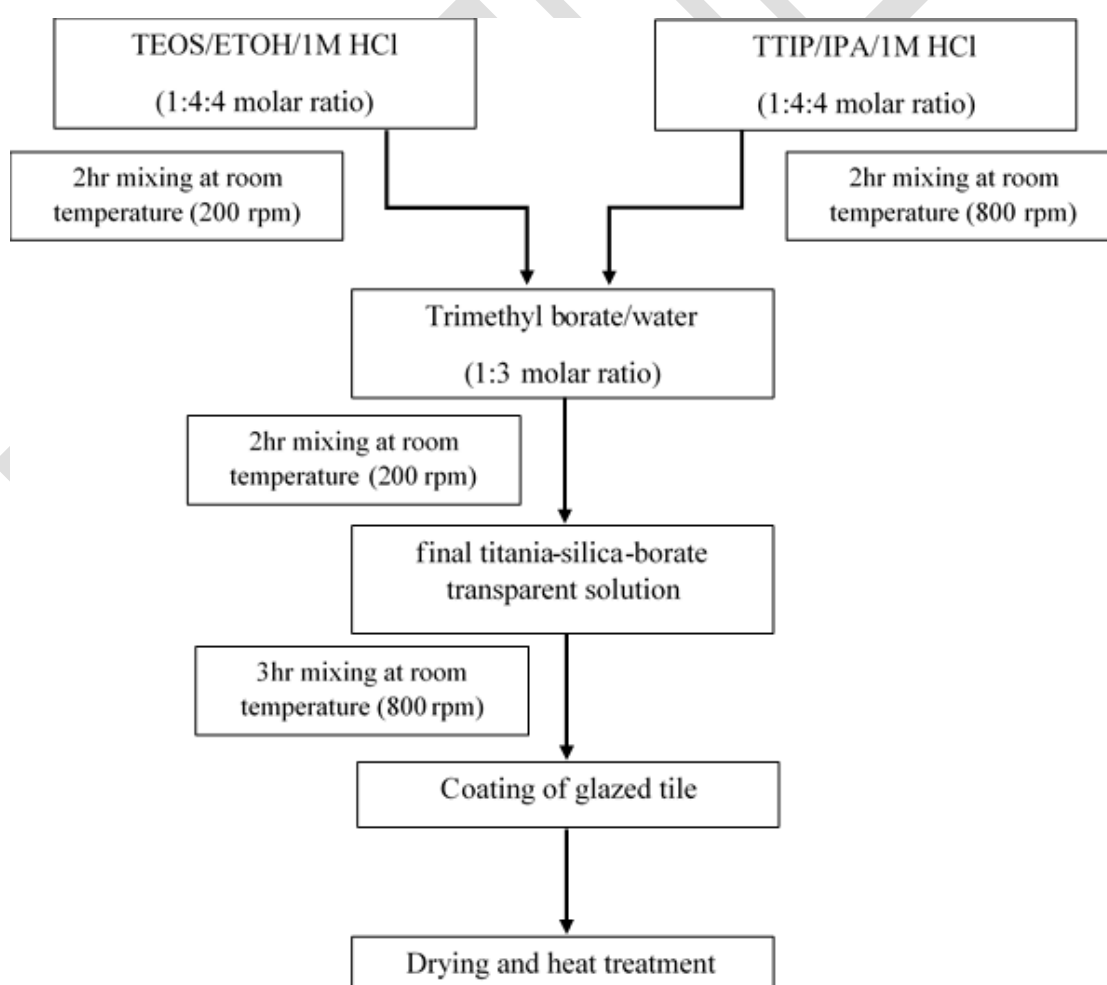


Fig.1. the flowchart of the glass ceramic coating preparation procedure.

2.3.Characterization techniques

Thermal behavior of the dried gels was studied by the Simultaneous Thermal Analysis (STA, TA Instruments Q600) in air and argo atmosphere. The heating rate was set at 10 °C/min and temperature ranged up to 900°C.

The crystallinity and the average crystallite size were determined by X-ray diffraction technique with Cu K α wavelength at 30 mA and 40 kV(XRD Bourevestnik Dron-8).

The microstructure of the resulted glass-ceramic coating layer was characterized by field emission scanning electron microscopy (FESEM, Mira 3-XMU) and scanning electron microscopy (SEM, TESCAN VWGAI) with an accelerating voltage of 15-20 kV. The surface of the samples was etched in 5% HF solution for 40 seconds before the test.

The photocatalytic activity was measured by the photo-degradation of Methylene Blue aqueous solution. Initial pollutant concentration was 10 micromolar, and the coated layer was irradiated by the UV source.

The MB removal efficiency was calculated by applying the Eq.(1):

$$\text{Removal efficiency(\%)} = [(C_0 - C) / C_0] \times 100 \quad (1)$$

Where C_0 and C are the initial and residual MB concentrations in the feed solution, respectively. Prior to the experiment, the sample was stored in a dark environment . subsequently, the samples were exposed to radiation to 1h and its absorbance was measured by the UV-Vis spectrophotometry, PerkinElmer, lambda 25, during this period.

3. Results and discussion

3.1. Thermal analysis of the sample

Figure 2 depicts the STA result of the dried ST-15B sample, taken in the air flow atmospher. Two distinct endothermic peaks on the DTA thermograph at around 70 °C and 190°C correspond to two weight reductions in the Tg thermograph. The observed endothermic peaks can be ascribed to the evaporation of mechanical water and rigid water from the sample. An exothermic peak occuring at around 270°C is caused by the oxidation of carbon groups. Moreover, as the test was conducted on the gel and prior to the heat treatment of the samples, there is no discernible peak reflecting crystallization.



Fig.2.STA thermograph of sample ST-15B in an air atmosphere

3.2. Crystallization behaviour

Figure 3 displays the X-ray diffraction (XRD) patterns of prepared samples following a 24-hour drying period at 150 °C. The observed pattern indicates that the dried gele exhibits an amorphous structure.

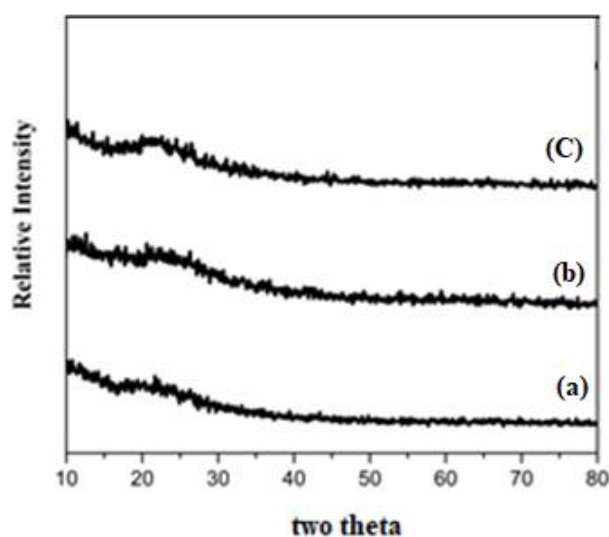


Fig 3. XRD pattern of the (a): ST-5B, (b): ST-10B and (C): ST-15B after drying at 150°C for 24 h.

Fig.4 presents the XRD patterns of sample ST-15B after calcination at 150 °C, 300 °C and 400 °C for 1 h. According to the figure, anatase formed in the gel, and crystallization increased as the temperature increased. The sample contains no evidence of rutile or brookite following the heat-treatment technique described above. The anatase phase peaks around $2\theta=25.3^\circ$ became sharper and more intense as the boron level increased.



Fig.4.XRD patterns of the ST-15B sample calcination at different temperatures.A: anatase

It should be noted that adding B_2O_3 to the coat composition instead of TiO_2 decreases the sintering temperature of coating [4]. Furthermore, it is claimed that adding boron to the crystalline structure of TiO_2 increases anatase thermal stability [5, 6]. The sintering of the layer improved with the boron oxide concentration, while the crystallinity of the coating steadily increased, despite the fact that the amount of titanium oxide in the coated layer gradually reduced. The XRD results as shown in figure 5, indicate that the addition of B_2O_3 to the TiO_2 system inhibits crystal growth and stabilizes the anatase phase, even at elevated temperatures. This behavior is consistent with previous findings in the literature and clearly verifies the significance of boron in the stability of anatase..

Mulmi et al. [24] reported that boron doping suppresses the growth of anatase crystals and maintains phase stability, as evidenced by their XRD patterns at room temperature. Similarly, Quesada-González et al. [25] found that the presence of boric acid during TiO_2 synthesis inhibited the rutile phase formation and promoted anatase phase stability.



Fig.5. The XRD pattern of samples after firing at 900°C for 1 h.

The crystallite size, lattice parameters, and the amounts of phases in the glass-ceramic layers fired at 900°C were determined using the Scherrer equation [5] and Rietveld refinement via Maud software. The statistical parameter SIG, reflecting the fit quality of the refinement, is also reported for each sample (Table 2).

Table 2. The crystallite size, unit cell dimensions, and the estimated amounts of various phases of the samples after firing at 900°C

| Sample | SIG | Phase | Unit Cell(A) | | Quantity of phases (wt.%) | The crystallite size(nm) |
|--------|--------|-----------|--------------|------|---------------------------|--------------------------|
| | | | a | C | | |
| ST-5B | 1.5054 | Anatase | 3.78 | 9.49 | 38 | 20 |
| | | Rutile | 4.55 | 2.90 | 2 | 100 |
| | | Amorphous | - | - | 60 | - |
| ST-10B | 1.4012 | Anatase | 3.79 | 9.51 | 54 | 21 |
| | | Rutile | 4.55 | 2.90 | 1.5-2 | 100 |
| | | Amorphous | - | - | 44 | - |
| ST-15B | 1.6494 | rutile | - | - | 0 | - |
| | | Anatase | 3.77 | 9.53 | 65 | 53 |
| | | Amorphous | - | - | 35 | - |

The results show that by increasing the amounts of boron oxide from 5 to 15 wt%, both the crystallite size and the amounts of anatase have increased. Previous studies report that the highest photocatalytic activity of an anatase coating has occurred with crystallite size in the

range of 8-10 nm that takes place after calcination below 500 °C. In this study, however, the size of the crystals has increase due to the force for increment the firing temperature of the coated layer. After considering all the criteria, sample ST-15B was selected for further study due to its high concentration of anatase crystalline phase and excellent surface quality following firing at 900 °C.

3.3. Microstructural studies

Figure 6 depict the FESEM images of the top views of the ST-15B glass-ceramic coated layer after being fired at 900°C for 1 hour. Surfaces with roughness and particles with uneven boundaries are detected. The coarse textures are a product of the HF etching procedure, which eliminates the remaining glassy phase and exposes more crystal particles on the surfaces. Due to the greater specific surface areas, this surface shape is regarded to be advantageous for improving the photocatalytic activity. The image shows that the anatase crystalline size is less than 65 nm, which accurately corresponds to the findings in Table 2.

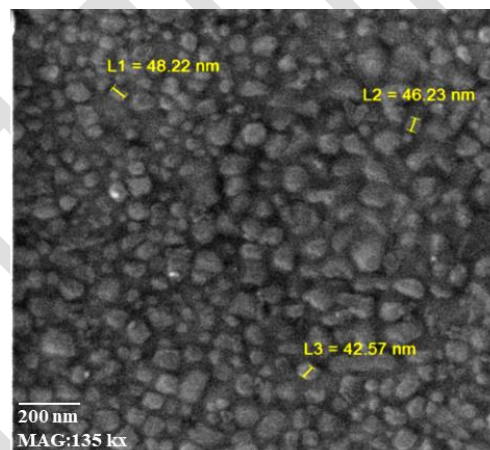


Fig.6. SEM micrographs of the ST-15B glass-ceramic

The cross-sectional view of the glaze-coated layer ST-15B interface is displayed in figure 7. As it can be observed, the coating exhibits a good adhesion to glaze. From these figs, the thickness of glaze and photocatalytic coatings are estimated 200 μm and 1.89μm respectively. These thicknesses are considered sufficient for coatings with satisfactory endurance.

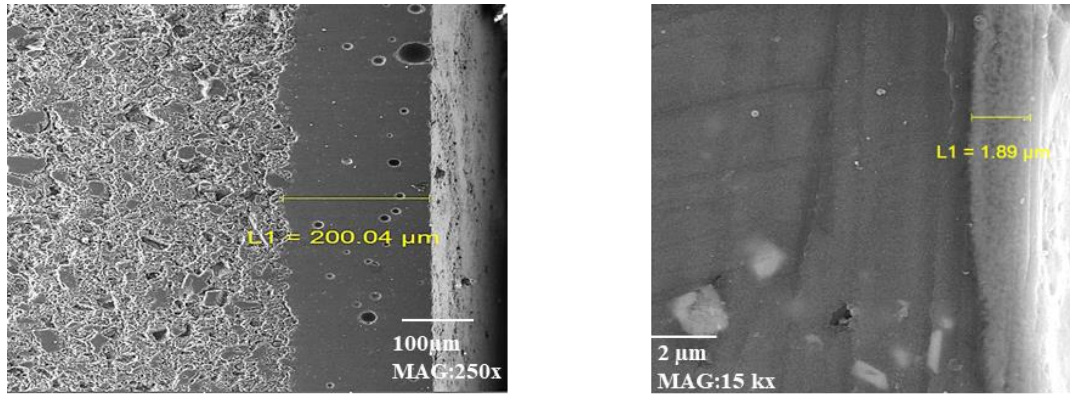


Fig.7. Cross-section of Photocatalyst coated glazed tile with ST-15B composition

3.4. photocatlytic properties

The photocatalytic property for samples were assessed by measuring the change in absorbance of MB solution under the UV radiation after exposition for 15 to 60 minutes, as depicted in figure 8.

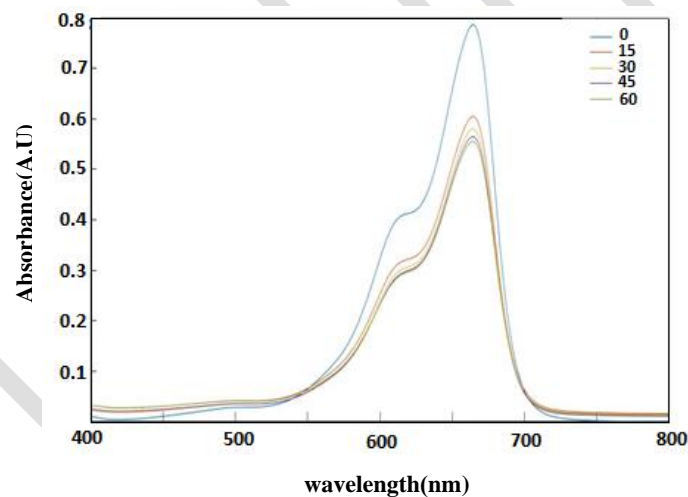


Fig. 8. Absorbance curves of MB aqueous solution in the presence of the ST-15B glass ceramic after UV-radiation.

According to the color degradation curve, degradation efficiency has improved with the radiation time. Actually, absorption decreases throughout the course of 60 minutes, and the degradation and decolorization process nears completion.

The photocatalytic activity observed in our study is largely attributed to the anatase phase of TiO_2 , which is well-known for its superior photocatalytic properties compared to the rutile and brookite phases. Anatase has a suitable band gap (~ 3.2 eV) that allows efficient absorption of UV light, resulting in the generation of electron-hole pairs (e^-/h^+) upon irradiation. Once excited, electrons in the valence band (VB) are promoted to the conduction band (CB), leaving behind holes in the VB:



These charge carriers can migrate to the surface of the catalyst where they participate in redox reactions. The photogenerated electrons reduce dissolved oxygen molecules to superoxide radicals ($\cdot\text{O}_2^-$), while the holes oxidize water or hydroxide ions to generate hydroxyl radicals ($\cdot\text{OH}$):



Both superoxide and hydroxyl radicals are highly reactive species capable of attacking and degrading organic dye molecules such as methylene blue into non-toxic byproducts like CO_2 and H_2O [26-27].

However, the photocatalytic efficiency can be affected by the recombination of e^-/h^+ pairs, which reduces the number of charge carriers available for surface reactions. Furthermore, the presence of other ions or compounds in solution can scavenge reactive species, leading to decreased degradation efficiency. As previously stated, the photocatalytic activity of the coating is dependent on the crystallinity and size of anatase crystals. Consequently it is evident that etching the glass ceramic prior to radiation can boost the photocatalytic activity of the synthesized coatings.

Conclusion:

Single phase transparent glass ceramic coating covering with photocatalytic property was successfully synthesized by heat treatment of sol-gel derived specimens in the $\text{TiO}_2\text{-B}_2\text{O}_3\text{-SiO}_2$ system. The following conclusions seem justified in light of the findings reported here:

- The addition of silica in the composition prevents anatase to rutile phase transformation even up to 900 °C.
- By increasing the boron oxide to the composition, viscosity of the system decreases, so the crystallinity of glass ceramic increases.
- with the increase of boron oxide from 5 to 15% by weight (in the constant weight percentage of silica), anatase crystallized in the system as single phase.
- Following 60 minutes of UV irradiation, the decomposition rate of methylene blue in the synthesized glass ceramic coating can reach up to 30%.

Reference

- [1] Rajesh Kumar, S., Suresh C., Vasudevan A.K., Suja N.R., Mukundan P. and Warriar K.G.K., "Phase transformation in sol-gel titania containing silica." *Mater. Lett.*, 1999, 38, 161-166.
- [2] Fujishima A., Zhang X. and Tryk D.A., "TiO₂ photocatalysis and related surface phenomena." *Surf. Sci. Rep.* 2008, 63, 515–82.
- [3] Tajer-Kajinebaf V., Sarpoolaky H. and Mohammadi T., "Sol-gel synthesis of nanostructured titania-silica mesoporous membranes with photo-degradation and physical separation capacities for water purification." *Ceram. Int.*, 2014, 40, 1747-1757.
- [4] Cheng P., Zheng M., Jin Y., Huang Q. and Gu M., "Preparation and characterization of silica-doped titania photocatalyst through the sol-gel method." *Mate. Lett.*, 2003, 57, 2989-2994.
- [5] Li Zh., Hou B., Xu Y., Wu D., Sun Y., Hu W. and Deng F., "Comparative study of sol-gel hydrothermal and sol-gel synthesis of titania-silica composite nanoparticles." *J. of solid state chem.*, 2005, 178, 1395-1405.
- [6] Bosc F., Ayrat A., Albouy P.A. and Guizard C., "A simple route for low- temperature synthesis of mesoporous and nanocrystalline anatase thin films." *Chem. Mat.*, 2003, 15, 2463–2468.
- [7] Jung K. Y., Park S. B. and Ihm S. K., "Local structure and photocatalytic activity of B₂O₃–SiO₂/TiO₂ ternary mixed oxides prepared by sol–gel method." *Appl. Catal. B: Environ.*, 2004, 51, 239-245.
- [8] Iordanova R., Gegova R., Bachvarova-Nedelcheva A. and Dimitriev Y., "Sol-gel synthesis of composites in the ternary TiO₂–TeO₂–B₂O₃ system." *Phys. Chem. Glasses: Eur. J. Glass Sci. Technol. B*, 2015, 56 (4), 128–138.
- [9] Moon S. C., Mametsuka H., Suzuki E., and Nakahara Y., "Characterization of titanium-boron binary oxides and their photocatalytic activity for stoichiometric decomposition of water." *Catal. Today*, 1998, 45, 79–84.
- [10] Jung K.Y. and Park S.B., "Anatase-phase titania: preparation by embedding silica and photocatalytic activity for the decomposition of trichloroethylene." *J. Photochem. Photobiol. A*, 1999, 127, 117–122.
- [11] Ijadpanah-Saravia H., Zolfagharib M., Khodadadic A. and Drogui P. "Synthesis, characterization, and photocatalytic activity of TiO₂–SiO₂ nanocomposites." *Desalin. Water Treat.*, 2016, 57, 14647–14655.

- [12] Anderson C. and Brad A.J., “Improved Photocatalytic Activity and Characterization of Mixed $\text{TiO}_2/\text{SiO}_2$ and $\text{TiO}_2/\text{Al}_2\text{O}_3$ Materials.” *J. Phys. Chem. B*, 1997, 101, 2611–2616.
- [13] Li Z., Hou B., Xu Y., Wu D. and Sun Y., “Hydrothermal synthesis, characterization, and photocatalytic performance of silica-modified titanium dioxide nanoparticles.” *J. Colloid Interface Sci.*, 2005, 149–154.
- [14] Bayram B., “Photocatalytic Activity of Titania–Silica Mixed Oxides Prepared with Co-Hydrolyzatio.”, M.S. Thesis in Chemical Engineering Department, Middle East Technical University.
- [15] Resende S. F., Gouveia R. L., Oliveira B. S., Vasconcelos W. L. and Augusti R., “synthesis of $\text{TiO}_2/\text{SiO}_2\text{-B}_2\text{O}_3$ Ternary Nanocomposites: Influence of Interfacial Properties on their Photocatalytic Activities with High Resolution Mass Spectrometry Monitoring.” *J. Braz. Chem. Soc.*, 2017, 28 (10), 1995–2003.
- [16] Bachvarova-Nedelcheva, A., Iordanova, R., Stoyanova, A., Georgieva, N., Nemska V. and Foteva T., “Effect of B_2O_3 on the Structure, Properties and Antibacterial Abilities of Sol-Gel-Derived $\text{TiO}_2/\text{TeO}_2/\text{B}_2\text{O}_3$ Powders.” *Materials*, 2023, 16, 6400.
- [17] Sciancalepore C. and Bondioli F., “Durability of $\text{SiO}_2\text{-TiO}_2$ photocatalytic coatings on ceramic tiles.” *Int. J. Appl. Ceram. Technol.*, 2015, 12, 679–684.
- [18] Fu J., “Highly photocatalytic glass ceramics containing $\text{MgTi}_4(\text{PO}_4)_6$ crystals.” *Mater. Lett.*, 2014, 118, 84–87.
- [19] Beall GH, Pinckney LR. Nanophase glass–ceramics. *J Am Ceram Soc* 1999;82: 5–16.
- [20] Masai H., Fujiwara T. and Mori H., “Fabrication of TiO_2 nanocrystallized glass.” *Appl. Phys. Lett.*, 2007, 90, 081907 (3).
- [21] Yazawa T., Machida F., Oki K., Mineshige A. and Kobune M., “Novel porous TiO_2 glass ceramics with highly photocatalytic ability.” *Ceram. Int.*, 2009, 35, 1693–7.
- [22] Fu J., “Photocatalytic properties of glass ceramics containing anatase-type TiO_2 .” *Mater. Lett.*, 2012, 68, 419–22.
- [23] Fu J., “Photocatalytic activity of glass ceramics containing Nasicon-type crystals.” *Mater. Res. Bull.*, 2013, 48, 70–3.
- [24] D. D. Mulmi, D. Thapa, B. Dahal, D. Baral, P. R. Solanki, “Spectroscopic Studies of Boron Doped Titanium Dioxide Nanoparticles.” *IJMSE*, 2016, 3, 172–178.
- [25] Cano-Casanova L., Ansón-Casaos A., Hernández-Ferrer J., Benito A. M., Maser W. K., Garro N., Lillo-Ródenas M. A. and, Román-Martínez M. C., “Surface-Enriched Boron-Doped TiO_2 Nanoparticles as Photocatalysts for Propene Oxidation.” *ACS Appl. Nano Mater.*, 2022, 5, 9, 12527–12539.

[26] Zhang J., Zhang Y., Leia Y. and Pan C., “*Photocatalytic and degradation mechanisms of anatase TiO₂: a HRTEM study.*”, *Catal. Sci. Technol.*, 2011, 1, 273–278.

[27] Desch N., Rheindorf A., Fassbender C., Slood M. and Lak M., “*Photocatalytic degradation of methylene blue by anatase TiO₂ coating.*” *Appl. Res.*, 2024, 3, e202300081.

